JNeuroscience

Research Articles: Systems/Circuits

A unifying motif for spatial and directional surround suppression

Liu D. Liu¹, Kenneth D. Miller² and Christopher C. Pack¹

¹Department of Neurology and Neurosurgery, Montreal Neurological Institute, McGill University, Montreal, Quebec H3A 2B4, Canada

²Department of Neuroscience, Center for Theoretical Neuroscience, Swartz Program in Theoretical Neuroscience, Kavli Institute for Brain Science, College of Physicians and Surgeons, Columbia University, New York, NY 10032, USA

DOI: 10.1523/JNEUROSCI.2386-17.2017

Received: 20 August 2017

Revised: 13 November 2017

Accepted: 2 December 2017

Published: 11 December 2017

Author contributions: L.D.L., K.D.M., and C.P. designed research; L.D.L. performed research; L.D.L. analyzed data; L.D.L., K.D.M., and C.P. wrote the paper.

Conflict of Interest: The authors declare no competing financial interests.

This work was supported by grants from the Canadian Institutes of Health Research to C.C.P. (PJT-148488) and L.D.L. (CGSD-121719), and NIH R01-EY11001 and the Gatsby Charitable Foundation (K.D.M.). We would like to thank Julie Coursol and the staff of the Animal Care Facility (Montreal Neurological Institute) for excellent technical support.

Corresponding author: Christopher C. Pack; christopher.pack@mcgill.ca; Montreal Neurological Institute, Montreal, Quebec H3A 2B4, Canada

Cite as: J. Neurosci ; 10.1523/JNEUROSCI.2386-17.2017

Alerts: Sign up at www.jneurosci.org/cgi/alerts to receive customized email alerts when the fully formatted version of this article is published.

Accepted manuscripts are peer-reviewed but have not been through the copyediting, formatting, or proofreading process.

Copyright © 2017 the authors

- <u>JNeurosci Accepted Manuscript</u>
- 1 Title: A unifying motif for spatial and directional surround suppression
- 2 Abbreviated title: Surround suppression in MT
- 3 Author names and affiliation: Liu D. Liu¹, Kenneth D. Miller², and Christopher C. Pack¹
- 4 ¹Department of Neurology and Neurosurgery, Montreal Neurological Institute, McGill
- 5 University, Montreal, Quebec H3A 2B4, Canada
- 6 ²Department of Neuroscience, Center for Theoretical Neuroscience, Swartz Program in
- 7 Theoretical Neuroscience, Kavli Institute for Brain Science, College of Physicians and Surgeons,
- 8 Columbia University, New York, NY 10032, USA
- 9 Corresponding author: Christopher C. Pack;
- 10 <u>christopher.pack@mcgill.ca;</u>
- 11 Montreal Neurological Institute, Montreal, Quebec H3A 2B4, Canada
- 12 Number of pages: 44
- 13 Number of figures: 7
- 14 Number of words for Abstract, Introduction, and Discussion: 245, 787, and 1487
- 15 **Conflict of interest:** The authors declare no competing financial interests.
- 16 Acknowledgements: This work was supported by grants from the Canadian Institutes of Health
- 17 Research to C.C.P. (PJT-148488) and L.D.L. (CGSD-121719), and NIH R01-EY11001 and the
- 18 Gatsby Charitable Foundation (K.D.M.). We would like to thank Julie Coursol and the staff of
- 19 the Animal Care Facility (Montreal Neurological Institute) for excellent technical support.

20 Abstract

21 In the visual system, the response to a stimulus in a neuron's receptive field can be modulated by 22 stimulus context, and the strength of these contextual influences vary with stimulus intensity. 23 Recent work has shown how a theoretical model, the stabilized supralinear network (SSN), can 24 account for such modulatory influences, using a small set of computational mechanisms. While 25 the predictions of the SSN have been confirmed in primary visual cortex (V1), its computational 26 principles apply with equal validity to any cortical structure. We have therefore tested the 27 generality of the SSN by examining modulatory influences in the middle temporal area (MT) of 28 the macaque visual cortex, using electrophysiological recordings and pharmacological 29 manipulations. We developed a novel stimulus that can be adjusted parametrically to be larger or 30 smaller in the space of all possible motion directions. We found, as predicted by the SSN, that 31 MT neurons integrate across motion directions for low-contrast stimuli, but that they exhibit 32 suppression by the same stimuli when they are high in contrast. These results are analogous to 33 those found in visual cortex when stimulus size is varied in the space domain. We further tested 34 the mechanisms of inhibition using pharmacologically manipulations of inhibitory efficacy. As 35 predicted by the SSN, local manipulation of inhibitory strength altered firing rates, but did not 36 change the strength of surround suppression. These results are consistent with the idea that the 37 SSN can account for modulatory influences along different stimulus dimensions and in different 38 cortical areas.

39 Significance Statement

40	Visual neurons are selective for specific stimulus features in a region of visual space known as
41	the receptive field, but can be modulated by stimuli outside of the receptive field. The SSN
42	model has been proposed to account for these and other modulatory influences, and tested in V1.
43	As this model is not specific to any particular stimulus feature or brain region, we wondered
44	whether similar modulatory influences might be observed for other stimulus dimensions and
45	other regions. We tested for specific patterns of modulatory influences in the domain of motion
46	direction, using electrophysiological recordings from MT. Our data confirm the predictions of
47	the SSN in MT, suggesting that the SSN computations might be a generic feature of sensory
48	cortex.

49 Introduction

50 What circuitry underlies sensory cortical processing? Recent work argues that visual 51 cortical circuitry is well described by a circuit termed the Stabilized Supralinear Network (SSN) 52 (Ahmadian et al., 2013; Rubin et al., 2015). The key idea is that neuronal gain – the change in 53 output per change in input – increases with activation. As a result, the effective connection 54 strengths between neurons increases with network activation, leading to a wide range of cortical 55 nonlinear behaviors.

One such behavior involves surround suppression: a decrease in a neuron's firing rate when the size of a stimulus exceeds that of the receptive field "center" (Allman et al., 1985; Jones et al., 2001; Cavanaugh et al., 2002). In the visual cortex, surround suppression is stronger for strong (high-contrast) stimuli than for weak (low-contrast) stimuli, so that the optimal stimulus size is larger for weaker stimuli (Sceniak et al., 1999; Pack et al., 2005; Tsui and Pack, 2011).

62 The SSN circuit explains this observation as follows. For very weak center stimuli, the 63 cortical region representing the center is weakly activated and has weak effective connection strengths. Therefore, monosynaptic inputs to the center from the surround, which are primarily 64 65 excitatory, dominate over di- and polysynaptic surround-driven local inputs, which are often 66 inhibitory. As a result, the surround stimulus facilitates the response. With increasingly strong 67 center activation, due either to a larger or higher-contrast stimulus, recurrent interactions become increasingly strong and increasingly inhibition-dominated (as observed in mouse V1, Adesnik 68 69 (2017)). The surround stimulus then more strongly drives inhibitory neurons, yielding surround 70 suppression. Thus, contrast-dependent surround suppression emerges from the dynamics of

recurrent activity, without the need for explicit assumptions about different contrast thresholds
for excitation and inhibition (Rubin et al., 2015).

73 Although the model has been primarily tested with V1 data, the underlying principles are 74 generic (Ozeki et al., 2009; Rubin et al., 2015; Miller, 2016). In particular, if the connection 75 strength between neurons decreases with their distance in a feature space (e.g., preferred 76 orientation in V1, (Cossell et al., 2015); or preferred direction in MT), then the SSN model 77 predicts that there should be contrast-dependent surround suppression in that feature space, just 78 as in retinotopic space (Rubin et al., 2015). MT should show such a decrease in connection 79 strength with increasing difference in preferred direction, because MT contains a local columnar 80 structure (Albright, 1984) so that nearby neurons encode similar motion directions (Born and 81 Bradley, 2005). The SSN thus predicts that MT neurons should show contrast-dependent 82 surround suppression in the space of motion-direction: stimuli that include a wider range of 83 motion directions, and thus activate MT neurons with a wider range of motion preferences, 84 should suppress MT responses; and this direction-domain suppression should be stronger at 85 higher contrasts and become weaker or absent at lower contrasts. Here we test this prediction in 86 monkey area MT.

We also test a second prediction. For reasonably strong activation, the excitatory recurrence becomes strong enough that the network becomes an inhibition-stabilized network (ISN): a network in which recurrent excitation is strong enough to be unstable (i.e., epileptic), but the network is stabilized by feedback inhibition (Tsodyks et al., 1997; Ozeki et al., 2009). An ISN shows a "paradoxical" response: when external excitatory drive is added to inhibitory cells (as when a surround stimulus drives center inhibitory cells sufficiently strongly to cause surround suppression), the inhibitory cells *lower* their sustained firing rates, due to loss of

94	recurrent excitation from suppressed excitatory cells. Thus, both excitatory and inhibitory cells
95	are surround suppressed, as assayed by the inhibition received by excitatory cells being reduced
96	by surround suppression (Ozeki et al., 2009; Adesnik, 2017). The SSN, and any model that is an
97	ISN, predicts that surround suppression is little affected by local blockade of GABAergic inputs
98	(Ozeki et al., 2004; Ozeki et al., 2009; Rubin et al., 2015), because the suppression is caused by a
99	withdrawal of excitatory input that is not disrupted by local manipulations of inhibition.
100	We tested the first prediction by designing a stimulus that could be manipulated
101	parametrically to be larger or smaller in the space of directions, while maintaining a fixed size in
102	visual space. We found that responses in MT were indeed suppressed by stimuli with a wider
103	range of motion directions, but only when the stimulus was high in contrast. At low contrast,
104	neurons integrated over a larger spread of motion directions, as has been observed for spatial
105	integration (Levitt and Lund, 1997; Kapadia et al., 1999; Sceniak et al., 1999). In addition, we
106	confirmed that local blockade of GABAergic inhibition does not reduce spatial surround
107	suppression in MT, just as in V1 (Ozeki et al., 2004). These results are consistent with the idea
108	that the SSN is a generic mechanism of cortical computation (Miller, 2016).

109 Materials and Methods

110 Electrophysiological Recordings and Visual Stimuli

- 111 Two adult female rhesus monkeys (*Macaca mulatta*, both 7 kg) were used for
- 112 electrophysiological recordings in this study. Before training, under general anesthesia, an MRI-
- 113 compatible titanium head post was attached to each monkey's skull. The head posts served to
- 114 stabilize their heads during subsequent training and experimental sessions. For both monkeys,
- 115 eye movements were monitored with an EyeLink1000 infrared eye tracking system (SR

116 Research) with a sampling rate of 1,000 Hz. All procedures conformed to regulations established

117 by the Canadian Council on Animal Care and were approved by the Institutional Animal Care

118 Committee of the Montreal Neurological Institute.

Area MT was identified based on an anatomical MRI scan, as well as depth, prevalence of direction-selective neurons, receptive field size to eccentricity relationship, and white matter to grey matter transition from a dorsal-posterior approach. We recorded single units using linear microelectrode arrays (V-Probe, Plexon) with 16 contacts.

Neural signals were thresholded online, and spikes were assigned to single units by a template-matching algorithm (Plexon MAP System). Offline, spikes were manually sorted using a combination of automated template matching, visual inspection of waveform, clustering in the space defined by the principle components, and absolute refractory period (1 ms) violations (Plexon Offline Sorter).

Visual motion stimuli were displayed at 60 Hz at a resolution of 1,280 by 800 pixels; the viewing area subtended $60^{\circ} \times 40^{\circ}$ at a viewing distance of 50 cm. Stimuli consisted of random dot stimuli displayed on a gray background (luminance of 98.8 cd/m²). Half the dots were black, and half the dots were white, resulting in a constant mean luminance across stimulus conditions.

At 100% contrast, the black dots had luminance of 0.4 cd/m^2 , and the white dots had luminance 132 of 198 cd/m². The intermediate contrasts were defined as a percentage of the luminance 133 difference from the gray background luminance, contrast = $|(\text{luminance} - 98.8 \text{ cd/m}^2)/98.8$ 134 cd/m^2 . Animals were trained to fixate on a small dot at the center of the screen. Stimuli were 135 136 shown after 300 ms of fixation. Each stimulus was presented for 500 ms, and the animals were 137 required to maintain fixation throughout the stimulus and for another 300 ms after the end of the 138 stimulus to receive a liquid reward. In all trials, gaze was required to remain within 2° of the 139 fixation point in order for the reward to be dispensed. Data from trials with broken fixation were 140 discarded.

The direction tuning and contrast response of the single units were quantified using 100% coherent dot patches placed inside the receptive fields. Offline the receptive field locations were further quantified by fitting a spatial Gaussian to the neuronal response measured over a 5 x 5 grid of stimulus positions. The grid consisted of moving dot patches centered on the initially hand-mapped receptive field locations. We confirmed that all neurons included in our analysis had receptive field centers within the stimulus patch used.

147

148 Size Tuning Stimuli in Direction Space

We designed a stimulus that would allow us to study surround suppression in the motion domain in a manner that was analogous to studies in the spatial domain. In this conception, the input to the receptive field "center" is the strength of motion in a range about the neuron's preferred direction. The "surround" is then motion in other directions, and the bandwidth of the center plus surround is the size of the stimulus in direction space. That is, a stimulus that contains motion in a range of directions spanning 180° is larger than a stimulus that spans a range of 60°. For these experiments we did not manipulate the spatial size of the stimulus, but rather fixed it accordingto the size of the hand-mapped spatial receptive field.

Our stimuli made use of random dots, each of which could be assigned to either a noise or a signal pool. The noise dots moved in random directions. The signal dots moved in a range of directions that straddled the preferred direction of each neuron. All dots moved at the same fixed speed of 8 or 16°/s, depending on the speed preference of the neuron. In all cases, dot patches were centered on the receptive fields determined by hand mapping. All conditions were interleaved randomly, and each stimulus was repeated 20 times.

We wished to change the size of the stimulus in direction space without changing other stimulus variables to which the neurons were sensitive. However, changing the size in direction space entails changing other low-level stimulus parameters (e.g., total number of dots or total amount of motion energy), which could confound our interpretation of the data. We therefore used two different methods to vary the stimulus bandwidth in direction space, each of which entailed changing a different low-level aspect of the stimulus.

169 In the first method, we kept the total number of stimulus dots fixed, and increased the 170 motion bandwidth by drawing dots from a noise pool. Thus the total number of dots was 171 identical for all stimuli, across variations in direction bandwidth. We constructed stimuli that 172 contained signal dots moving in 1, 3, 5, and 7 directions, and each increase in the number of 173 motion directions involved recruiting 25% of the noise dots to move coherently in the new 174 direction (Fig. 1A and Table 1). This paradigm thus allowed us to test the influence of size in 175 direction space for stimuli comprised of a fixed number of dots and a fixed amount of overall 176 motion energy. We limited the largest size in direction space to be ±90° from the preferred

direction in order to avoid null direction suppression at larger sizes (Snowden et al., 1991; Qianand Andersen, 1994).

179 However, in this approach, increases in motion bandwidth are yoked to decreases in 180 noise, which might be expected to affect the strength of inhibitory inputs on their own (Hunter 181 and Born, 2011). Thus, we also tested neurons using a second method, in which there was no 182 noise pool, and we increased the size in direction space by simply adding more dots that moved 183 in different directions. In this case the center stimulus strength (i.e. the strength of motion in the 184 preferred direction) was constant across conditions, but the total number of dots (and hence the 185 total motion energy) increased with stimulus size. The lowest dot density used was 2 dots/degree², which is beyond the density at which MT responses typically saturate, at least for 186 187 100% coherence stimuli (Snowden et al., 1992). We again tested four different direction 188 conditions (Fig. 1B and Table 1). In all cases, the dot size was 0.1°. The dots were initially 189 plotted at random locations and moved in fixed directions from frame to frame. A dot that left 190 the patch was replotted at the corresponding location on the opposite boundary of the patch on 191 the next frame and continued its motion from there, i.e. the lifetime was equal to the stimulus 192 duration (Qian and Andersen, 1994).

Number of	Method 1: varying the noise pool, with		arying the noise pool, with Method 2: varying the dot density	
directions	dot density fixed to 2 dots/degree ² (Fig		without adding any n	oise dots (Fig
	1A)		1B)	
	Signal directions	Noise	Directions	Density
1	25% at preferred direction	75%	Preferred direction	2 dots/degree^2
3	25% at preferred; 25% at $\pm 30^{\circ}$	50%	Preferred; ±30°	4 dots/degree ²
	from preferred		from preferred	

5	25% at preferred; 25% at $\pm 30^{\circ}$	25%	Preferred; $\pm 30^{\circ}$ and	6 dots/degree ²
	and 25% at $\pm 60^{\circ}$ from preferred		±60° from preferred	
7	25% at preferred; 25% at $\pm 30^{\circ}$;	0%	Preferred; ±30°,	8 dots/degree ²
	25% at $\pm 60^{\circ}$; and 25% at $\pm 90^{\circ}$		$\pm 60^\circ$ and $\pm 90^\circ$ from	
	from preferred		preferred	

193 **Table 1.** Summary of the two methods of stimulus generation.

194

For all size tuning experiments in direction space, we tested each of the 4 sizes at high and low contrasts. High contrast was defined as 100% contrast, and the low contrast was chosen online to be around the c_{50} of the contrast response function obtained with the 100% coherent dot patch. Offline, we eliminated one neuron for which the response at the lowest contrast was below 2 standard deviations of the spontaneous baseline firing rate.

200

204

201 Grating, plaid, and pattern selectivity

202 We tested a subset of MT neurons (n = 65) with a standard measure of motion integration, the 203 plaid stimulus (Movshon et al., 1985). Direction selectivity for each neuron was first measured

with a 100% contrast drifting sinusoidal grating of spatial frequency of 0.5 cycles/^o. Stimulus

size and temporal frequency were matched to the neuron's preferences. Plaid stimuli were

206 constructed by superimposing two gratings (Fig. 5A).

We used the standard approach to quantify the component and pattern selectivity of each
neuron (Smith et al., 2005). The partial correlations for the pattern and component predictions
were calculated as,

$$PC_p = \frac{r_p - r_c r_{pc}}{\sqrt{(1 - r_c^2)(1 - r_{pc}^2)}}$$

$$PC_{c} = \frac{r_{c} - r_{p}r_{pc}}{\sqrt{(1 - r_{p}^{2})(1 - r_{pc}^{2})}}$$

210 Here, r_p and r_c are the correlations between the plaid response and the pattern and component

211 predictions, respectively, and r_{pc} is the correlation between the pattern and component

212 predictions. The partial correlations are z-scored as,

$$Z_p = 0.5ln\left(\frac{(1 + PC_p)/(1 - PC_p)}{\sqrt{1/(n-3)}}\right)$$
$$Z_c = 0.5ln\left(\frac{(1 + PC_c)/(1 - PC_c)}{\sqrt{1/(n-3)}}\right)$$

213 Where n = 12 is the number of directions. The pattern index was calculated as $Z_p - Z_c$.

214

215 Pharmacological Injections

216 The pharmacological injection system has been previously described (Liu and Pack, 2017).

217 Briefly, our linear electrode arrays contained a glass capillary with an inner diameter of 40 µm.

218 One end of the capillary was positioned at the opening between contacts 5 and 6 of the array

219 (contact 1 was most dorsal-posterior), so that the separation of the injection site from the

220 recording contacts ranged between 0 and 1000 µm. The other end of the capillary was connected

221 via plastic tubing to a Hamilton syringe for the injection of pharmacological agents with a

222 minipump.

223 To effectively manipulate neuronal responses without compromising isolation, we

224 typically used injections of 0.1-0.2 μ L at 0.05 μ L/min. For GABA, we used a concentration of

225 25 mM, which reduced neural activity without silencing it completely (Bolz and Gilbert, 1986;

- 226 Nealey and Maunsell, 1994). For gabazine, the concentration was 0.05 mM, and we used
- 227 injections of approximately 0.5 µL at 0.05 µL/min. In a few cases, this induced unstable and

228 synchronized responses in the nearby neurons (Chagnac-Amitai and Connors, 1989). The

230

231 Data Analysis

MT direction tuning curves $r(x_d)$ were characterized by fitting a Gaussian function to the mean responses using the least-squares minimization algorithm (lsqcurvefit in MATLAB). The

234 Gaussian function is

235 $r(x_d) = ae^{-0.5d(\theta, x_d)^2/b^2} + m$

where a scales the height of the tuning curve; b determines the tuning curve width, the direction

tuning width (DW) was defined as full width at half maximum of the fit, i.e. 2.35b; x_d is the

238 motion direction; θ is the preferred direction of motion; and *m* is the baseline firing rate of the

239 cell. $d(\theta, x_d)$ is the shortest distance around the 360 degree circle between θ and x_d . The Gaussian

240 fit to the data was very good in most cases (Median $R^2 = 0.90$ before gabazine injection and $R^2 =$

241 0.89 after injection).

242 The contrast response functions $r(x_c)$ were fitted with a Naka-Rushton function,

$$r(x_c) = R_{max} \frac{x_c^n}{x_c^n + c_{50}^n} + m$$

where R_{max} scales the height of the contrast response function; *n* determines the slope; c_{50} is the contrast at which the response function achieves half of its maximum response; and *m* is the baseline firing rate of the cell. x_c is the contrast.

246 The neuronal size tuning curves $r(x_s)$ in retinotopic space were fitted by a Difference of 247 Error functions (DoE) (Sceniak et al., 1999; DeAngelis and Uka, 2003),

$$r(x_s) = A_e erf\left(\frac{x_s}{s_e}\right) - A_i erf\left(\frac{x_s}{s_e + s_i}\right) + m$$

where A_e and A_i scale the height of the excitatory center and inhibitory surround, respectively. s_e and s_i are the excitatory and inhibitory sizes, and *m* is the baseline firing rate of the cell. x_s is the stimulus size. The DoE fit to the data was very good in most cases (Median R² = 0.93 before gabazine injection and R² = 0.93 after injection).

The size suppression index (SI_s) for each neuronal size tuning curve was calculated as SI_S = $(R_m - R_L)/R_m$, where R_m is the maximum across responses to different stimulus sizes and R_L is the response observed at the largest size. Since using the raw responses is sensitive to noise at both the maximum response and the response at the largest size, we used the values from the DoE fits for SI calculations.

Since we only measured the response at 4 sizes in the directional space, we were unable to fit a DoE function to the directional size tuning curves. Instead, to capture potential suppressive influences in the direction domain, we calculated a direction integration index from the raw data $II_D = (R_L - R_S) / (R_L + R_S)$, where R_L is the response observed at the largest size and R_S is the response observed at the smallest size.

262

263 SSN Model Simulations

We first simulated a 1D ring model, which captures putative interactions among neurons

265 representing different motion directions (Fig. 2A). Details of this model can be found elsewhere

266 (Rubin et al., 2015). Our model differs in that the ring is 360 degrees in extent (vs. 180 degrees

267 in Rubin et al., 2015), representing all possible motion directions. There is an excitatory (E) and

268 inhibitory (I) neuron at every integer position $x_i = 0^\circ, 1^\circ, \dots, 359^\circ$, where x_i represents the

269 preferred direction of the corresponding E and I cells. We can write the model equation in matrix

270 notation as,

271
$$\tau \frac{d}{dt} \boldsymbol{r}(x_i) = -\boldsymbol{r}(x_i) + k([\boldsymbol{W}^* \boldsymbol{r}(x_i) + c\boldsymbol{h}(x_i)]_+)^n$$

272 where $r(x_i)$ is the vector of firing rates of the excitatory and inhibitory neurons with preferred 273 motion direction x_i , W(y) is the weight matrix of $E \to E$, $E \to I$, $I \to E$, and $I \to I$ connections 274 between neurons separated by angular distance y (measured as shortest distance around the 360° 275 circle). The connection weights $W_{ab}(y) = J_{ab}G\sigma_{dir}(y)$, where $J_{EE} = 0.044$, $J_{EI} = 0.023$, $J_{IE} = 0.042$, 276 $J_{II} = 0.018$, $G\sigma_{dir}(y)$ are a Gaussian function with standard deviation of 64° (Ahmadian et al., 2013). $W^*r(x_i)$ is the convolution $\sum_j W(x_i - x_j)r(x_j)$ 277 where the sum is over all preferred 278 directions x_i ; $h(x_i)$ is the vector of external input to the E and I neurons preferring x_i ; and c is 279 the strength (monotonically related to contrast) of the input. The elements of the vector of input 280 to the neuron, $W^*r(x_i) + ch(x_i)$, are thresholded at zero before being raised to the power n: $[z]_+ = 0$ if z < 0, = z if $z \ge 0$ (the operations of thresholding and raising to a power are 281 282 applied separately to each element of the vector). k and n are identical for E and I neurons, with k = 0.04 and n = 2. τ is a diagonal matrix of the time constant for E cells, $\tau_{\rm E} = 20$ ms, and for I 283 cells, $\tau_{\rm I} = 10$ ms. 284 285 Regarding the model parameter choices, the four amplitudes Jab were constrained to 286 ensure stability and strong nonlinear behavior. To ensure stability, we require $J_{EI}J_{IE} > J_{EE}J_{II}$,

287 meaning feedback inhibition is sufficiently strong. For equal-strength inputs to E and I cells as

288 used here, the strongest nonlinear behavior also requires $J_{II}-J_{EI} < 0$ and $J_{II}-J_{EI} < J_{IE}-J_{EE}$

(Ahmadian et al., 2013). We chose $G\sigma_{dir}(y)$ to have a standard deviation of 64°, given the

bandwidth of MT direction tuning curves and the idea that cells with more strongly overlapping tuning curves should more strongly connect to each other; this value can be varied to give a diversity of surround suppression as observed in the data. We chose n = 2 for the power-law

293 input-output (I/O) function, consistent with the observation in V1 that neurons have I/O

functions well described by a power law throughout the full range of firing induced by visual stimuli, with powers in the range 2-5 (Priebe and Ferster, 2008). At n = 2, k =0.04 gave reasonable firing rates, but the qualitative behavior is consistent for a large range of n and k. Finally, we chose the ratio of the time constants for E and for I cells, $\tau_E/\tau_I = 2$, to help ensure stability; given that the network is stable, the time constants do not affect the steady-state network responses, which is what we are modeling here.

300 We simulated network responses to random dot field stimuli of variable coherence. We 301 assumed that a coherent dot stimulus of a given direction gives input to MT neurons proportional 302 to a Gaussian function, of standard deviation 60°, of the difference (shortest distance around a 303 360° circle) between the neuron's preferred direction and the stimulus direction. To simulate the 304 method using noise dots (Table 1, Method 1), the non-coherent (noise) dots gave equal input, 305 proportional to 1/360, to neurons of all preferred directions. The strength of the stimulus is given 306 by a parameter c, identified as the "contrast" in Figure 2. As in our electrophysiological 307 experiments, we used stimuli corresponding to 4 different sizes in direction space (Fig. 1A). 308 Thus for the smallest size, 25% of the input, **h**, was modelled as a Gaussian distribution around 309 the preferred direction (peak of the Gaussian = c/4), while the remaining 75% was spread equally 310 around the ring (uniform distribution of size $(3/4) \times c/360$). At 2 directions, an additional 25% 311 was taken from the non-coherent input and added to Gaussian spreads about +/-30° from the 312 preferred direction (these two Gaussians have peak = c/8; noise amplitude becomes (1/2) × 313 c/360). 3 and 4 directions followed in a similar manner while the total input strength was kept 314 constant across sizes. We also simulated Method 2 (Table 1), which used the same set of stimuli 315 except without a noise background (so that the total input strength grew with increasing number 316 of directions), and the results were qualitatively similar as presented in Results.

- <u>JNeurosci Accepted Manuscript</u>
- 317

318 Experimental design and statistical analysis

319 We used two female rhesus monkeys (Macaca mulatta) for electrophysiological recordings in 320 this study; this is standard for electrophysiological studies involving monkeys. We used the 321 Wilcoxon rank-sum test to evaluate the difference between the Integration Index at low and high 322 contrast, and the difference between Direction Tuning Width and Suppression Index before and 323 after injection of Gabazine. As the Direction Tuning Width and Suppression Index can be 324 affected by the ability to sample the tuning curves, we performed a bootstrapping analysis to 325 ensure the robustness of the summary statistics. For each cell, we randomly sampled (with 326 replacement) 10 trials per direction or size to create a tuning curve and then fitted a circular 327 Gaussian or DoE to the subsampled tuning curve to generate a new direction tuning width or 328 suppression index. We generated 100 sample distributions and tested the effects of gabazine 329 injections with a Wilcoxon signed-rank test. To evaluate the relationship between the Pattern 330 Index and Direction Tuning Width and the Integration Index, we calculated Pearson correlation 331 coefficients. All analyses made use of built-in MATLAB functions and custom scripts. The 332 complete results of the statistical analyses for each experiment can be found in the corresponding 333 Results section.

335	In this section, we first present simulation results for the SSN. We then test a crucial model
336	prediction with neurophysiological recordings from MT neurons in awake and behaving
337	macaques. The theoretical and empirical results show that surround suppression in the motion
338	domain behaves similarly to surround suppression in the space domain, with integration at low
339	contrasts switching to suppression at high contrasts (Figs. 3 and 4). We also find that pattern-
340	selective cells (as assayed from plaid responses) show greater motion integration than
341	component-selective cells (Fig. 5). Finally, as predicted by the SSN model, local
342	pharmacological manipulation of inhibition does not alter spatial surround suppression, although
343	our methods had the expected effects on directional tuning width (Figs. 6 and 7).
344	
345	Stabilized supralinear network predicts contrast-dependent surround suppression in the
346	direction domain in MT
346 347	<i>direction domain in MT</i> Previous instantiations of the SSN have considered a model in which connections are defined
347	Previous instantiations of the SSN have considered a model in which connections are defined
347 348	Previous instantiations of the SSN have considered a model in which connections are defined either across a retinotopic sheet of the kind found in V1 or across a ring of preferred orientations
347 348 349	Previous instantiations of the SSN have considered a model in which connections are defined either across a retinotopic sheet of the kind found in V1 or across a ring of preferred orientations (Ahmadian et al., 2013; Rubin et al., 2015; Miller, 2016). Like orientation, motion direction is a
347348349350	Previous instantiations of the SSN have considered a model in which connections are defined either across a retinotopic sheet of the kind found in V1 or across a ring of preferred orientations (Ahmadian et al., 2013; Rubin et al., 2015; Miller, 2016). Like orientation, motion direction is a circular variable, but it takes values over 360° rather than 180° as for orientation. Thus to
347348349350351	Previous instantiations of the SSN have considered a model in which connections are defined either across a retinotopic sheet of the kind found in V1 or across a ring of preferred orientations (Ahmadian et al., 2013; Rubin et al., 2015; Miller, 2016). Like orientation, motion direction is a circular variable, but it takes values over 360° rather than 180° as for orientation. Thus to examine the properties of the SSN in this circular space, we first simulated a ring model ((Rubin
 347 348 349 350 351 352 	Previous instantiations of the SSN have considered a model in which connections are defined either across a retinotopic sheet of the kind found in V1 or across a ring of preferred orientations (Ahmadian et al., 2013; Rubin et al., 2015; Miller, 2016). Like orientation, motion direction is a circular variable, but it takes values over 360° rather than 180° as for orientation. Thus to examine the properties of the SSN in this circular space, we first simulated a ring model ((Rubin et al., 2015); Fig. 2A) of motion direction space. This represents neurons of varying preferred
 347 348 349 350 351 352 353 	Previous instantiations of the SSN have considered a model in which connections are defined either across a retinotopic sheet of the kind found in V1 or across a ring of preferred orientations (Ahmadian et al., 2013; Rubin et al., 2015; Miller, 2016). Like orientation, motion direction is a circular variable, but it takes values over 360° rather than 180° as for orientation. Thus to examine the properties of the SSN in this circular space, we first simulated a ring model ((Rubin et al., 2015); Fig. 2A) of motion direction space. This represents neurons of varying preferred directions sharing a common location in retinotopic space.

357	them. We accordingly assumed that the strengths of connections between neurons on the ring
358	decreased with increasing difference in their preferred directions. By analogy with the study of
359	size-tuning in the spatial domain, we tested the SSN with stimuli of different motion-domain
360	sizes. We increased the size of the stimulus in direction space by including stimuli at
361	increasingly wider ranges of directions about the preferred direction (the "center" of the
362	receptive field). As described in Methods, we considered size or bandwidth 0° (preferred-
363	direction stimulus only), 60° (adding stimuli at +/- 30° about the preferred), 120° (adding
364	additional stimuli at +/- 60°), and 180° (additional stimuli at +/- 90°). For each motion size, we
365	examined different levels of stimulus contrast, represented as scaling the strengths of all inputs.
366	The simulation results (Fig. 2B) show that the model predicts strong direction-domain
367	surround suppression at high contrast, but not at low contrast. Specifically, at low contrasts (red),
368	increasing the range of motion directions leads to increased responses with a hint of suppression
369	for the largest stimulus size, while at high contrasts larger motion-domain stimulus sizes lead to
370	strong suppression (blue). Intermediate contrasts give an intermediate result (black). These
371	results change very little with changes in the total number of dots in the stimulus (Fig. 2C), a
372	factor that we consider in our experiments below (Fig. 4). Thus the model consistently predicts
373	direction-domain suppression that is analogous to space-domain surround suppression. In the
374	SSN, the dependence of surround suppression on contrast arises generically from the dynamics
375	of the SSN in summing inputs, rather than by the assumption of a higher contrast threshold for
376	inhibition, as in previous models (Somers et al., 1998; Huang et al., 2008; Schwabe et al., 2010;
377	Carandini and Heeger, 2012).
378	

380 Surround suppression in direction domain of MT

381 We tested the model predictions by recording from individual MT neurons, using the same 382 stimuli as in the simulations. We first show results for the first type of stimulus described above, 383 in which there was a noise pool of dots moving in random directions. For each neuron we fixed 384 the physical size of each stimulus according to an estimate of the classical receptive field size. 385 We then varied stimulus size in the motion domain, as well as dot contrast. Thus for the smallest 386 stimulus, all the coherent dots moved in the preferred direction of the neuron (Fig. 1A, left), with 387 the remaining dots in the noise pool moving in random directions. To increase the size of stimuli 388 in the motion space, we recruited dots from the noise pool and added them to directions around 389 the preferred direction (Fig. 1A). This manipulation kept the total motion energy and dot density 390 of the stimulus constant across sizes.

391 Figure 3A shows the firing rate of an example MT neuron for stimuli of different 392 contrasts and motion sizes. For the low contrast stimulus (red), firing rate increased with motion 393 size, while for higher contrasts (blue, black) firing rate decreased with motion size. Thus the 394 pattern of firing rates for this neuron was consistent with the SSN prediction that MT neurons 395 would shift from motion-domain integration to suppression as the stimulus contrast was 396 increased (Fig. 3A). Indeed, just as in the space domain, for large stimuli it is possible to increase 397 firing rates by lowering contrast (Fig. 3A; Pack et al., 2005). 398 To examine these effects across the MT population, we calculated the directional 399 integration index (II_D, the difference between responses to the largest and smallest sizes divided

400 by the sum of these responses; see Methods) for data of the kind shown in Figure 3A for 125

401 neurons. The II_D captures the integration of signals across motion directions, with larger II_D

402 values indicating more integration. Across the population (Fig. 3C) the II_D was frequently below

403 zero, indicating a suppression of the response when dots activated the directional surround. 404 Overall the II_D was significantly decreased at high contrast compared to low contrast, consistent 405 with reduced integration at high contrasts (p < 0.001, rank sum test; p < 0.001 for monkey 1 and 406 p = 0.01 for monkey 2). Note that this is not due to a failure of the low contrast stimuli to elicit a 407 response from the neurons, as all neurons except one showed responses to the lowest contrast 408 tested that were significantly above baseline. The one neuron that failed to meet this criterion 409 was eliminated from further analysis. Overall, these results are similar to previous results in the 410 space domain in MT (Pack et al., 2005; Tsui and Pack, 2011). However, the mechanisms of 411 spatial and directional integration for a given cell appeared to be independent, as there was no 412 correlation between the degree of spatial surround suppression and directional surround 413 suppression measured at high contrast in the same neurons (Pearson's r = -0.06, p = 0.46, N = 414 124). 415 We also tested 46 neurons using a second stimulus in which there was no noise pool, and

416 we increased the total number of stimulus dots with size in the direction domain (Fig. 1B). This 417 stimulus was designed to control for a potential confound in the previous experiment, which kept 418 the total number of dots constant across stimulus size. In the latter configuration, increases in 419 direction-domain size were yoked to decreases in the number of noise dots, and because noise 420 includes motion in all directions, this can be viewed as reduction in the strength of the directional 421 surround, analogous to the far surround in retinal space (Angelucci and Bullier, 2003; Angelucci 422 and Bressloff, 2006). The new stimulus was directly analogous to that typically used in size 423 tuning experiments, in which the stimulus is simply expanded to probe the influence of the 424 surround.

We tested this subpopulation of MT neurons with both stimuli, and the results are shown in Figures 4A and 4B. For the control stimulus, the II_D is still significantly higher at low contrast than at high contrast (Fig. 4A; p = 0.04, rank sum test). Thus integration across direction space was greater at low contrast, regardless of how size was manipulated. For these neurons, we also replicated the previous result using the stimulus with a constant total number of dots (Fig. 4B; p< 0.001, rank sum test). The contrast modulation of II_D was not significantly different for the two stimulus types (rank sum test, p = 0.45).

432 Of the complete MT population, 65 were also tested with a standard probe of direction-433 domain integration, the plaid stimulus (Movshon et al., 1985). Our plaid stimuli consisted of two 434 superimposed sine-wave gratings, moving in directions separated by 120° (Fig. 5A); stimulus 435 size was again matched to the classical receptive field, and contrast was 100%. From the 436 resulting data we computed a pattern index (see Methods; Smith et al., 2005), which captures the 437 extent to which MT neurons integrate the two motion directions; higher values indicate greater 438 integration (Fig. 5B and C). We found that the pattern index was significantly correlated with the 439 directional II_D, as measured in our direction-size-tuning experiments at both low (Fig. 5D; 440 Pearson's r = 0.33, p = 0.01) and high contrasts (r = 0.27, p = 0.03). That is, cells with higher 441 pattern indices showed less surround suppression in direction space - greater motion integration 442 -- both at low and high stimulus contrasts. This suggests that area MT might use similar 443 mechanisms to integrate motion signals for dot stimuli and grating stimuli. We also found that 444 there was no correlation between the directional motion integration index and the width of the 445 direction tuning curve, as measured using responses to standard stimuli of drifting dots moving 446 coherently in a single direction (Fig. 5E; Pearson's r = -0.08, p = 0.38 for low contrast, r = 0.05, 447 p = 0.57 for high contrast).

448 *GABAergic influence on neuronal direction tuning and surround suppression in the spatial*

449 domain

450 Another prediction of the SSN is that local changes in the strength of inhibition should have little 451 or no effect on surround suppression, because surround suppression is a result of withdrawal of 452 network excitation (as well as inhibition), and a local blockade of inhibition will not change 453 these network dynamics (Ozeki et al., 2009). This is different from conventional models, which 454 posit that suppression is induced by an increase in the inhibition that a cell receives, so that a 455 reduction in the inhibition to a given neuron will reduce its surround suppression (Tsui and Pack, 456 2011). Previous work has confirmed the SSN predictions in anesthetized cat V1, using 457 iontophoretic injection of GABA antagonists: inhibitory blockade did not reduce surround 458 suppression (Ozeki et al., 2004). In this section, we examine the effects of pharmacological 459 manipulation of GABA in MT of awake monkeys.

We first confirmed that gabazine, a GABA_A receptor antagonist, robustly modulated neuronal firing in MT (Thiele et al., 2012). We measured direction tuning using random-dot stimuli of fixed spatial size, with all dots moving coherently in a single direction (Fig. 6A). We found that injection of gabazine increased direction tuning width, as found previously (Thiele et al., 2004; Thiele et al., 2012). In contrast, injections of GABA decreased firing rates across all directions (Fig. 6E), leading to narrower tuning (Leventhal et al., 2003).

Figure 7A summarizes the influence of gabazine on direction tuning widths for a population of 38 MT cells: Tuning width increased following the injection, as determined by a rank sum test (p = 0.04) and verified with a bootstrapping analysis (see Methods; Wilcoxon signed-rank test; p < 0.001); these increases were particularly noticeable for cells that were

470 narrowly tuned before the injection, as noted previously in V1 of anesthetized cat (Katzner et al.,

471 2011). These changes in tuning width were not associated with changes in spontaneous firing 472 rate, as the changes in spontaneous were modest and did not reach statistical significance (rank 473 sum test, p = 0.32). Moreover, there was no correlation between gabazine-induced changes in 474 spontaneous firing and changes in tuning width (Pearson's r = 0.05, p = 0.78). We did not have 475 enough data from the GABA experiments to perform statistical analyses, but in all 5 476 experiments, direction tuning width decreased following injection. 477 To test the influence of GABA concentrations on surround suppression, we performed 478 standard (space-domain) measurements of size tuning, using random-dot stimuli (100%

coherence) of different physical extents, with all dots moving in the neuron's preferred direction
(Fig. 6B). Previous work has shown that these stimuli elicit surround suppression in the upper
and lower layers in MT, but not in layer 4, suggesting that the suppression is generated through
intrinsic connections within MT (Born and Tootell, 1992; Raiguel et al., 1995). This property
makes such stimuli useful for testing the predicted role of inhibitory inputs in the SSN.

484 Figure 6D shows size tuning curves from the same MT neuron as in Figure 6C. The pre-485 injection data (black line) show that the neuron exhibited substantial surround suppression, as the 486 response was reduced significantly with increasing stimulus size. As for the direction tuning 487 curve, injection of gabazine increased firing rates in a non-specific manner. However, in this 488 neuron there was no apparent reduction in surround suppression (Fig. 6D), and this result was 489 generally true for the MT population (n = 38): The size suppression index (SI₈), defined as the 490 difference between the peak response and the response to the largest stimulus divided by the 491 peak response, was similar before and after injection of gabazine (Fig. 7B; rank sum test, p =0.98; bootstrapping analysis followed by Wilcoxon signed-rank test; p = 0.99). Again there was 492 493 no correlation between the effects of gabazine on SI and the effects on spontaneous firing

494	(Pearson's $r = -0.11$, $p = 0.52$). These results are similar to those found in V1 of anesthetized cats
495	(Ozeki et al., 2004), despite the much larger volume of gabazine used here. In a smaller sample
496	(n = 5), we found that injection of GABA did not increase surround suppression, despite a strong

497 overall reduction in firing rate (Fig. 6F).

498 Discussion

499 Through electrophysiological recordings in awake monkeys, we have found contrast-dependent 500 surround suppression in MT in a space defined by motion directions. In addition, we found that 501 local manipulation of the efficacy of GABAergic inhibition had little influence on standard 502 measures of surround suppression. Both results are consistent with predictions of the stabilized 503 supralinear network (SSN), previously tested in V1 (Rubin et al., 2015). 504 505 SSN as a unifying motif for normalization in multiple cortical areas 506 The contrast dependence of surround suppression in the space domain has been observed in both 507

507 V1 and MT (Polat et al., 1998; Kapadia et al., 1999; Sceniak et al., 1999; Pack et al., 2005;

508 Schwabe et al., 2010; Tsui and Pack, 2011). These results have previously been modeled under

509 the assumption that inhibitory neurons have higher contrast thresholds than excitatory neurons

510 (Somers et al., 1998; Huang et al., 2008; Schwabe et al., 2010; Carandini and Heeger, 2012).

511 However, there is little experimental support for this assumption, and some data that contradict it

512 (Contreras and Palmer, 2003; Song and Li, 2008).

513 In the SSN, the excitatory and inhibitory units can have the same properties (Rubin et al., 514 2015). Each unit has a power-law input/output function, but is stabilized by network inhibition 515 (Ozeki et al., 2009; Ahmadian et al., 2013; Rubin et al., 2015). With low contrast inputs, the 516 recurrent interactions within the network are weak, so neurons act relatively independently, 517 summing their feedforward inputs and responding according to their transfer functions. With 518 higher-contrast inputs, strong recurrent connections within the network provide contrast- and 519 size-dependent suppression, with size in the spatial and feature (direction) domains playing 520 similar roles.

The SSN also predicts that the local blockade of GABA_A receptors should not reduce surround suppression (Ozeki et al., 2009). In the SSN, surround suppression is not a result of an increase in inhibitory GABAergic input, but a withdrawal of both excitation and inhibition. In contrast, in models in which surround suppression results from an increase in the inhibition received by suppressed neurons (e.g., Tsui and Pack, 2011), local blockade of inhibition should reduce or prevent surround suppression.

527 Modulatory influences in visual cortex are often modeled within the normalization 528 framework, which is hypothesized to be a generic computation with equal validity across brain 529 regions and stimulus modalities (Carandini et al., 1997; Reynolds and Heeger, 2009; Carandini 530 and Heeger, 2012; Krause and Pack, 2014). The normalization model as typically conceived, is a 531 phenomenological rather than circuit model, in which some form of unnormalized neuronal 532 response is suppressed by the sum of unnormalized responses in other neurons that constitute the "normalization pool". The precise form of normalization, for example whether the normalizing 533 534 pool constitutes all neurons or is restricted in some way based on neuronal tuning, must be 535 matched to fit the particular experiments modeled. 536 The SSN can be regarded as a circuit instantiation of the normalization model, in that

many SSN results closely match the results of an appropriately constructed normalization model (Rubin et al., 2015). In the circuit implementation, the form of normalization is determined by the connectivity. For example, in the SSN, orientation-specific long-range horizontal connectivity leads to the orientation-selectivity of surround suppression (Rubin et al., 2015); in a normalization model, this would be explained by assuming that the normalization pool consists of neurons of similar preferred orientations to the normalized cell. The normalization model does not explain the mechanism of suppression, and alternative mechanisms yield different predictions. For example, if the normalization pool exerted suppression by adding inhibition to the normalized cells, then one would expect increased inhibition and increased conductance in normalized (e.g., surround-suppressed) cells, and local GABAergic blockade would reduce or eliminate the normalization. In the SSN mechanism, normalization typically results from a decrease in both excitation and inhibition and thus a decreased conductance (Rubin et al., 2015).

550 Relationship to motion integration in MT

In MT, the integration of different motion directions has frequently been probed with the plaid stimuli (Movshon et al., 1985; Smith et al., 2005), comprised of superimposed gratings moving in different directions. Previous work has distinguished between pattern cells, which respond to the plaid motion direction, and component cells, which respond to the individual grating motion directions (Movshon et al., 1985).

In the terminology used here, a plaid stimulus moving in a neuron's preferred direction entails component motion confined to the directional surround. Thus for a high-contrast plaid, the component gratings should suppress the neuron's response, and this could contribute to the observed responses of component neurons. Furthermore, component-selective neurons have small direction centers (i.e. narrow tuning width), so that they do not integrate input from two gratings moving in very different directions (Rust et al., 2006; Tsui et al., 2010; Khawaja et al., 2013).

Pattern cells have broader direction tuning than component cells (Rust et al., 2006;
Khawaja et al., 2013). Direction tuning, measured from the responses to individual motion
directions, corresponds to the "minimal response field" in visual space, the region in which small
stimuli can activate the cell; this measure does not change with contrast (Song and Li, 2008). Our

567	measure of motion integration is not correlated with direction tuning width (Fig. 5E), and is best
568	related to the "summation field size" in visual space, the size of a stimulus that best drives a cell
569	before further size increases cause surround suppression. The summation field size, like our
570	measure of motion integration, shrinks with contrast (Sceniak et al., 1999). We found a weak
571	correlation between our motion integration index and the pattern index, which quantifies
572	integration of plaid stimuli (Fig. 5D). These results suggest that the motion-domain summation
573	field and pattern selectivity are linked, but that summation on its own is insufficient to account
574	for pattern selectivity.
575	Pattern cells also show stronger suppression than component cells by stimuli moving
576	opposite to their preferred directions (Rust et al., 2006). This suggests a direction-domain
577	analogue of the "far surround" suppression that is found in the space domain; such suppression is
578	also regulated by contrast both in the direction domain in MT (Pack et al., 2005) and in spatial
579	surrounds in V1 (Schwabe et al., 2010). Our stimuli did not contain null-direction motion, and so
580	they would not have probed this component of the MT receptive fields. Nevertheless, an
581	inference from the existing data is that pattern cells in MT have both larger directional
582	summation fields and larger (or stronger) directional surrounds.
583	It can be argued that random-dot stimuli are larger than gratings in the direction domain,
584	as they activate a broader range of columns in V1 (Simoncelli and Heeger, 1998). Thus stimuli
585	composed of multiple dots fields moving in different directions might elicit stronger suppression
586	than grating stimuli containing a similar number of directions. Evidence in support of this idea

587 comes from studies that use transparent motion stimuli, comprised of overlapping dot fields

588 moving in two different directions. These stimuli evoke responses in MT that seem to reflect a

suppression of responses to stimuli that straddle the preferred direction (Xiao and Huang, 2015),

particularly for pattern cells (McDonald et al., 2014). One prediction of the current work is that
such suppression should be weaker for low-contrast stimuli.

592

593 Functional correlates of integration and suppression

594 A number of psychophysical studies have drawn a close link between contrast-dependent

595 responses in MT and visual motion perception. For simple motion discrimination tasks,

596 performance mirrors spatial processing in MT: for high-contrast stimuli, performance is worse

597 for large than for small stimuli (Tadin et al., 2003; Liu et al., 2016). Similarly, motion perception

598 can decrease at high contrasts when the stimulus speed is low, mirroring the contrast-dependent

599 suppression found in MT (Pack et al., 2005; Seitz et al., 2008). In the direction domain, MT

600 neurons exhibit higher null-direction suppression when the stimulus is high in contrast (Pack et

al., 2005). This suggests further that suppressive influences are stronger for high-contrast stimuli,

and there is some evidence that motion perception can worsen as the size of the stimulus

603 increases in the direction domain (Treue et al., 2000; Dakin et al., 2005). Conversely, motion

discrimination with noisy dots can sometimes improve at low contrast (Tadin et al., 2003). Our

605 results predict the ability to integrate motion signals in the direction domain should

606 systematically improve at low contrast, as has been found with manipulations of stimulus speed

607 (Seitz et al., 2008) and spatial size (Tadin et al., 2003).

608

609 Conclusion

610 A growing body of evidence points to a set of generic computations that are similar across brain

611 regions (Creutzfeldt, 1977; Barlow, 1985; Miller, 2016) and across sensory modalities

612 (Mountcastle, 1978; Pack and Bensmaia, 2015). Although this idea is attractive from a

- 613 theoretical standpoint, it remains somewhat speculative. In this work, we have provided an
- 614 experimental test of the genericity of one computational model by comparing results in MT with
- 615 those obtained previously in V1. The qualitative pattern of results is similar, supporting the
- 616 possibility that this model provides a more general framework for modulatory responses and
- 617 integration in cortex.

References Adesnik H (2017) Synaptic Mechanisms of Feature Coding in the Visual Cortex of Awake Mice. Neuron 95:1147-1159 e1144. Ahmadian Y, Rubin DB, Miller KD (2013) Analysis of the stabilized supralinear network. Neural Comput 25:1994-2037. Albright TD (1984) Direction and orientation selectivity of neurons in visual area MT of the

- 625 macaque. J Neurophysiol 52:1106-1130.
- 626 Allman J, Miezin F, McGuinness E (1985) Stimulus specific responses from beyond the classical
- 627 receptive field: neurophysiological mechanisms for local-global comparisons in visual neurons.
- 628 Annu Rev Neurosci 8:407-430.

618

619 620

621

622

623

- 629 Angelucci A, Bullier J (2003) Reaching beyond the classical receptive field of V1 neurons:
- 630 horizontal or feedback axons? J Physiol Paris 97:141-154.
- 631 Angelucci A, Bressloff PC (2006) Contribution of feedforward, lateral and feedback connections
- to the classical receptive field center and extra-classical receptive field surround of primate V1
- 633 neurons. Prog Brain Res 154:93-120.
- 634 Barlow HB (1985) The twelfth Bartlett memorial lecture: the role of single neurons in the
- 635 psychology of perception. Q J Exp Psychol A 37:121-145.
- 636 Bolz J, Gilbert CD (1986) Generation of end-inhibition in the visual cortex via interlaminar
- 637 connections. Nature 320:362-365.
- 638 Born RT, Tootell RB (1992) Segregation of global and local motion processing in primate
- 639 middle temporal visual area. Nature 357:497-499.
- Born RT, Bradley DC (2005) Structure and function of visual area MT. Annu Rev Neurosci
 28:157-189.

- 642 Carandini M, Heeger DJ (2012) Normalization as a canonical neural computation. Nat Rev
- 643 Neurosci 13:51-62.
- 644 Carandini M, Heeger DJ, Movshon JA (1997) Linearity and normalization in simple cells of the
- 645 macaque primary visual cortex. Journal of Neuroscience 17:8621.
- 646 Cavanaugh JR, Bair W, Movshon JA (2002) Nature and interaction of signals from the receptive
- 647 field center and surround in macaque V1 neurons. J Neurophysiol 88:2530-2546.
- 648 Chagnac-Amitai Y, Connors BW (1989) Horizontal spread of synchronized activity in neocortex
- and its control by GABA-mediated inhibition. J Neurophysiol 61:747-758.
- 650 Contreras D, Palmer L (2003) Response to contrast of electrophysiologically defined cell classes
- 651 in primary visual cortex. J Neurosci 23:6936-6945.
- 652 Cossell L, Iacaruso MF, Muir DR, Houlton R, Sader EN, Ko H, Hofer SB, Mrsic-Flogel TD
- 653 (2015) Functional organization of excitatory synaptic strength in primary visual cortex. Nature654 518:399-403.
- 655 Creutzfeldt OD (1977) Generality of the functional structure of the neocortex.
- 656 Naturwissenschaften 64:507-517.
- 657 Dakin SC, Mareschal I, Bex PJ (2005) Local and global limitations on direction integration
- assessed using equivalent noise analysis. Vision Res 45:3027-3049.
- 659 DeAngelis GC, Uka T (2003) Coding of horizontal disparity and velocity by MT neurons in the
- alert macaque. J Neurophysiol 89:1094-1111.
- 661 Huang X, Albright TD, Stoner GR (2008) Stimulus dependency and mechanisms of surround
- 662 modulation in cortical area MT. J Neurosci 28:13889-13906.
- 663 Hunter JN, Born RT (2011) Stimulus-dependent modulation of suppressive influences in MT. J
- 664 Neurosci 31:678-686.

- Jones HE, Grieve KL, Wang W, Sillito AM (2001) Surround suppression in primate V1. J
- 666 Neurophysiol 86:2011-2028.
- 667 Kapadia MK, Westheimer G, Gilbert CD (1999) Dynamics of spatial summation in primary
- visual cortex of alert monkeys. Proc Natl Acad Sci U S A 96:12073-12078.
- Katzner S, Busse L, Carandini M (2011) GABAA inhibition controls response gain in visual
 cortex. J Neurosci 31:5931-5941.
- 671 Khawaja FA, Liu LD, Pack CC (2013) Responses of MST neurons to plaid stimuli. J
- 672 Neurophysiol 110:63-74.
- 673 Krause MR, Pack CC (2014) Contextual modulation and stimulus selectivity in extrastriate
- 674 cortex. Vision Res 104:36-46.
- 675 Leventhal AG, Wang Y, Pu M, Zhou Y, Ma Y (2003) GABA and its agonists improved visual
- 676 cortical function in senescent monkeys. Science 300:812-815.
- 677 Levitt JB, Lund JS (1997) Contrast dependence of contextual effects in primate visual cortex.
- 678 Nature 387:73-76.
- 679 Liu LD, Pack CC (2017) The Contribution of Area MT to Visual Motion Perception Depends on
- 680 Training. Neuron 95:436-446 e433.
- Liu LD, Haefner RM, Pack CC (2016) A neural basis for the spatial suppression of visual motion
 perception. Elife 5.
- 683 McDonald JS, Clifford CW, Solomon SS, Chen SC, Solomon SG (2014) Integration and
- segregation of multiple motion signals by neurons in area MT of primate. J Neurophysiol111:369-378.
- 686 Miller KD (2016) Canonical computations of cerebral cortex. Curr Opin Neurobiol 37:75-84.
- 687 Mountcastle VB (1978) Brain mechanisms for directed attention. J R Soc Med 71:14-28.

- 688 Movshon JA, Adelson EH, Gizzi MS, Newsome WT (1985) The analysis of visual moving
- 689 patterns. In: Pattern Recognition Mechanisms (Chagas C, Gattass R, Gross C, eds), pp 117-151.
- 690 New York: Springer.
- 691 Nealey TA, Maunsell JH (1994) Magnocellular and parvocellular contributions to the responses
- 692 of neurons in macaque striate cortex. J Neurosci 14:2069-2079.
- 693 Ozeki H, Finn IM, Schaffer ES, Miller KD, Ferster D (2009) Inhibitory stabilization of the
- 694 cortical network underlies visual surround suppression. Neuron 62:578-592.
- 695 Ozeki H, Sadakane O, Akasaki T, Naito T, Shimegi S, Sato H (2004) Relationship between
- 696 excitation and inhibition underlying size tuning and contextual response modulation in the cat
- 697 primary visual cortex. J Neurosci 24:1428-1438.
- Pack CC, Bensmaia SJ (2015) Seeing and Feeling Motion: Canonical Computations in Vision
 and Touch. PLoS Biol 13:e1002271.
- 700 Pack CC, Hunter JN, Born RT (2005) Contrast dependence of suppressive influences in cortical
- area MT of alert macaque. J Neurophysiol 93:1809-1815.
- 702 Polat U, Mizobe K, Pettet MW, Kasamatsu T, Norcia AM (1998) Collinear stimuli regulate
- visual responses depending on cell's contrast threshold. Nature 391:580-584.
- Priebe NJ, Ferster D (2008) Inhibition, spike threshold, and stimulus selectivity in primary visual
 cortex. Neuron 57:482-497.
- 706 Qian N, Andersen RA (1994) Transparent motion perception as detection of unbalanced motion
- 707 signals. II. Physiology. J Neurosci 14:7367-7380.
- 708 Raiguel S, Van Hulle MM, Xiao DK, Marcar VL, Orban GA (1995) Shape and spatial
- 709 distribution of receptive fields and antagonistic motion surrounds in the middle temporal area
- 710 (V5) of the macaque. Eur J Neurosci 7:2064-2082.

- Reynolds JH, Heeger DJ (2009) The normalization model of attention. Neuron 61:168-185.
- 712 Rubin DB, Van Hooser SD, Miller KD (2015) The stabilized supralinear network: a unifying
- 713 circuit motif underlying multi-input integration in sensory cortex. Neuron 85:402-417.
- 714 Rust NC, Mante V, Simoncelli EP, Movshon JA (2006) How MT cells analyze the motion of
- 715 visual patterns. Nat Neurosci 9:1421-1431.
- Sceniak MP, Ringach DL, Hawken MJ, Shapley R (1999) Contrast's effect on spatial summation
 by macaque V1 neurons. Nat Neurosci 2:733-739.
- 718 Schwabe L, Ichida JM, Shushruth S, Mangapathy P, Angelucci A (2010) Contrast-dependence of
- 719 surround suppression in Macaque V1: experimental testing of a recurrent network model.
- 720 Neuroimage 52:777-792.

711

- 721 Seitz AR, Pilly PK, Pack CC (2008) Interactions between contrast and spatial displacement in
- visual motion processing. Curr Biol 18:R904-906.
- Simoncelli EP, Heeger DJ (1998) A model of neuronal responses in visual area MT. Vision Res
 38:743-761.
- Smith MA, Majaj NJ, Movshon JA (2005) Dynamics of motion signaling by neurons in macaque
 area MT. Nat Neurosci 8:220-228.
- 727 Snowden RJ, Treue S, Andersen RA (1992) The response of neurons in areas V1 and MT of the
- alert rhesus monkey to moving random dot patterns. Exp Brain Res 88:389-400.
- 729 Snowden RJ, Treue S, Erickson RG, Andersen RA (1991) The response of area MT and V1
- neurons to transparent motion. J Neurosci 11:2768-2785.
- 731 Somers DC, Todorov EV, Siapas AG, Toth LJ, Kim DS, Sur M (1998) A local circuit approach
- to understanding integration of long-range inputs in primary visual cortex. Cereb Cortex 8:204-

733 217.

- 734 Song XM, Li CY (2008) Contrast-dependent and contrast-independent spatial summation of
- primary visual cortical neurons of the cat. Cereb Cortex 18:331-336.
- 736 Tadin D, Lappin JS, Gilroy LA, Blake R (2003) Perceptual consequences of centre-surround
- antagonism in visual motion processing. Nature 424:312-315.
- 738 Thiele A, Distler C, Korbmacher H, Hoffmann KP (2004) Contribution of inhibitory
- 739 mechanisms to direction selectivity and response normalization in macaque middle temporal
- 740 area. Proc Natl Acad Sci U S A 101:9810-9815.
- 741 Thiele A, Herrero JL, Distler C, Hoffmann KP (2012) Contribution of cholinergic and
- 742 GABAergic mechanisms to direction tuning, discriminability, response reliability, and neuronal
- rate correlations in macaque middle temporal area. J Neurosci 32:16602-16615.
- 744 Treue S, Hol K, Rauber HJ (2000) Seeing multiple directions of motion-physiology and
- 745 psychophysics. Nat Neurosci 3:270-276.
- 746 Tsodyks MV, Skaggs WE, Sejnowski TJ, McNaughton BL (1997) Paradoxical effects of
- external modulation of inhibitory interneurons. J Neurosci 17:4382-4388.
- 748 Tsui JM, Pack CC (2011) Contrast sensitivity of MT receptive field centers and surrounds. J
- 749 Neurophysiol 106:1888-1900.
- 750 Tsui JM, Hunter JN, Born RT, Pack CC (2010) The role of V1 surround suppression in MT
- 751 motion integration. J Neurophysiol 103:3123-3138.
- 752 Xiao J, Huang X (2015) Distributed and Dynamic Neural Encoding of Multiple Motion
- 753 Directions of Transparently Moving Stimuli in Cortical Area MT. J Neurosci 35:16180-16198.
- 754

755

<u>JNeurosci Accepted Manuscript</u>

756 Figure Legends

757

Figure 1. Illustration of the two methods of stimulus generation. A, Illustration of the stimulus
that engages directional surround suppression in MT while the dot density is fixed. B, Illustration
of the stimulus that engages directional surround suppression in MT while the dot density
increases with directional size.

762

763 Figure 2. Stabilized supralinear network can account for surround suppression in both spatial 764 and direction domains. A, Schematic of the 1D SSN ring model as a direction space analogue of 765 the visual space model. In the visual space model (top), stimuli of different sizes in visual space 766 (gray circles) are simulated as input, h(x), of varying width, to a linear 1D grid of excitatory (E, 767 red) and inhibitory (I, blue) units. The grid positions represent visual space positions. In the 768 direction space (bottom), there are 360 E and I units, with coordinates on the ring as preferred 769 directions. A dot stimulus, h(x), moving at a single direction is a Gaussian-shaped input with 770 standard deviation of 60°. Stimuli including multiple directions simply add such input for each 771 direction. We considered two methods of adding directions: including a "noise pool" stimulus of 772 equal input to all directions, and subtracting from the noise pool as we added directions to keep 773 total input strength unchanged (Fig. 1A); or simply adding additional input as we added 774 directions, without a noise pool (Fig. 1B). B, Directional surround suppression at high contrast, 775 but not at low contrast, arises from the dynamics of the model. This simulation result is for the 776 first method of taking dots from a noise pool to add further directions about the preferred (Fig. 777 1A). The response at each contrast is normalized to the peak response. C, The simulation result

778 for the second method of adding dots to further directions about the preferred without a noise

pool (Fig. 1B). The response at each contrast is normalized to the peak response.

780

781 Figure 3. Surround integration and suppression in the direction domain. A, Surround

suppression occurs in direction space at high contrast, but not at low contrast for an example neuron. **B**, Contrast response function for the same example neuron using 100% coherent dots in the preferred direction. The line indicates the Naka-Rushton function fit. **C**, Population data for direction surround integration. Scatter plot of the integration index, II_D , at low contrast against the II_D at high contrast (rank sum test, p < 0.001). The marginal distributions are histograms of the II_D (Median at high contrast = 0.002; Median at low contrast = 0.084). Dashed lines in the histograms show location of $II_D = 0$.

789

790 Figure 4. Additional controls for direction surround integration and suppression. A, Population 791 data for direction surround integration. Scatter plot of the directional integration index (II_D) at 792 low contrast against the II_D at high contrast (rank sum test, p = 0.04). The marginal distributions 793 are histograms of the II_D (Median at high contrast = -0.012; Median at low contrast = 0.018). 794 Dashed lines in the histograms show location of $II_D = 0$. **B**, The contrast modulation of II_D for the 795 same 46 neurons as in B, when the number of dots is held fixed by drawing from a noise pool (as 796 in Fig. 3). The conventions are the same as in panel B (Median at high contrast = 0.003; Median 797 at low contrast = 0.065).

798

Figure 5. Direction integration with plaid stimuli. A, Illustration of the grating (left) and plaid
stimuli (right). B, Direction tuning curve for an example neuron in response to drifting gratings.

801 **C**, Direction tuning curve for the same neuron in response to moving plaids. The dashed line 802 indicates the component prediction, which is the expected result if the neuron fails to integrate 803 the motion of the plaid. **D**, Population data for motion integration. Scatter plot of the pattern 804 index against the directional integration index (II_D) at low contrast (r = 0.33, p = 0.01). **E**, Scatter 805 plot of the direction tuning width against the directional integration index (II_D) at low contrast (r = 0.38).

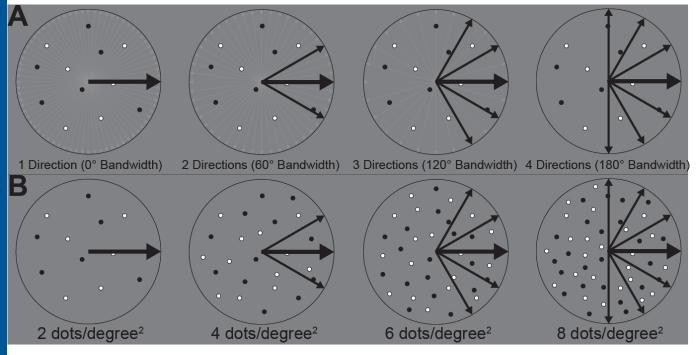
807

808 Figure 6. Effect of GABA on motion direction and size tuning. A and B, 100% coherent random 809 dot patches were used to probe the direction and size tuning of MT neurons. C and E, Direction 810 tuning curve for an example neuron before (black) and after injection of gabazine (C, red) or 811 GABA (E, blue). The points are the mean responses for each direction. The lines indicate 812 Gaussian function fits. Direction tuning width (DW) was defined as full width at half maximum 813 of the fit. **D** and **F**, Size tuning curves for an example neuron, plotting the firing rate (mean \pm 814 s.e.m.) as a function of patch size before (black) and after injection of gabazine (D, red) or 815 GABA (F, blue). The lines indicate difference of error functions fits. The horizontal lines show 816 the spontaneous firing rate.

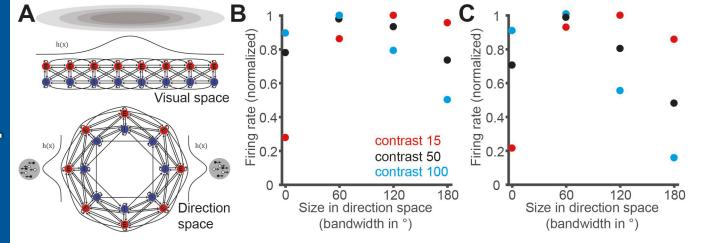
817

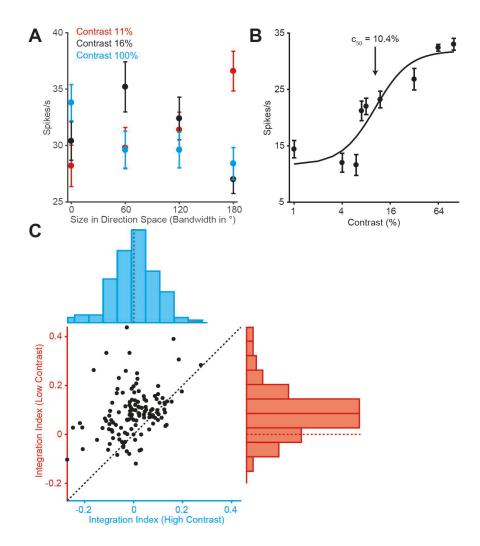
Figure 7. Population data on the effects of gabazine on direction and size tuning. A, Scatter plot of the direction tuning width before the injection of gabazine against the tuning width after injection (rank sum test, p = 0.04). Red and black lines represent the medians of the respective marginal distributions. **B**, Scatter plot of the neuronal size suppression index (SI_S) before the injection of gabazine against the neuronal SI_S after injection (rank sum test, p = 0.98).

JNeurosci Accepted Manuscript



JNeurosci Accepted Manuscript





JNeurosci Accepted Manuscript

